Southern Hemisphere Forecast Experiments with a One-Level Spectral Model

BRYANT J. MCAVANEY AND WILLIAM BOURKE

Australian Numerical Meteorology Research Centre, Melbourne, Victoria, 3001

(Manuscript received 13 May 1974, in revised form 3 March 1975)

ABSTRACT

A one-level primitive equation spectral model has been initialized with hemispheric 500 mb geopotential height and vorticity fields using the Southern Hemisphere GARP data sets for the period 3–12 November 1969 inclusive. Experiments performed to choose values of the external parameters of the model showed that resolution up to wavenumber 15 and a mean free surface height of 5.6 km were suitable for 48 h prognoses. The distributions with respect to both latitude and planetary wavenumber in the mean square error were determined for the model prognoses. Over the mid-latitude range 30°S to 60°S and over the wavenumber range 3 to 9, 48 h prognoses proved consistently better than persistence.

1. Introduction

Although hemispheric prognoses have been regularly computed in the Northern Hemisphere for almost two decades the situation in the Southern Hemisphere is greatly different. Owing to the major limitation of the sparsity of data in the Southern Hemisphere relatively fewer hemispheric numerical forecast experiments have been conducted. In particular, a detailed evaluation of hemispheric barotropic prognoses in the Southern Hemisphere does not appear to be available in the literature, although an evaluation of a limited-area barotropic model has been made for the Australian region (Voice *et al.*, 1972). The present study was prompted by the availability of an efficient hemispheric one-level spectral model (Bourke, 1972), coupled with access to the Southern Hemisphere portion of the GARP basic data set analyses for the special observing period of November 1969; the main purpose of this study was to evaluate the quality of the prognoses produced by this spectral model for the Southern Hemisphere.

2. Prediction model

The formulation of the model used in this study has been fully described by Bourke (1972, hereafter designated by I); however, for ease of subsequent discussion the relevant equations of motion and spectral representations are repeated here. The set of equations used describe the motion of the free surface of a shallow, homogeneous, incompressible fluid layer on a rotating sphere; the prognostic variables are the vertical component of relative vorticity (ζ), the horizontal divergence (D), and the geopotential height (Φ). Equations (10), (11) and (12) of Bourke's paper, with a modification to allow for bottom topography, are relevant and are as follows:

$$\frac{\partial\zeta}{\partial t}=-\frac{1}{a\cos^2\phi}\left[\frac{\partial}{\partial\lambda}(U\zeta)+\cos\phi\frac{\partial}{\partial\phi}(V\zeta)\right]-2\Omega\left(\sin\phi D+\frac{V}{a}\right), \quad (1)$$

$$\frac{\partial D}{\partial t}=\frac{1}{a\cos^2\phi}\left[\frac{\partial}{\partial\lambda}(V\zeta)-\cos\phi\frac{\partial}{\partial\phi}(U\zeta)\right]+2\Omega(\sin\phi\zeta-U/a)-\nabla^2\left(\frac{U^2+V^2}{2\cos^2\phi}+\Phi'\right), \quad (2)$$

$$\frac{\partial\Phi}{\partial t}=-\frac{1}{a\cos^2\phi}\left\{\frac{\partial}{\partial\lambda}[U(\Phi'-\Phi_s')]+\cos\phi\frac{\partial}{\partial\phi}[V(\Phi'-\Phi_s')]\right\}-(\bar{\Phi}-\bar{\Phi}_s)D, \quad (3)$$

where the notation is identical to that in I but with the addition of terms containing Φ_s, the geopotential height of the earth's surface.

The spatial variations in relative vorticity, divergence and geopotential are approximated by truncated expansions in spherical harmonics. These expansions[1] are

[1] The vorticity and divergence spectral amplitudes (ζ_l^m and D_l^m) defined by these expansions are related to the streamfunction and velocity potential amplitudes in I (ψ_l^m and χ_l^m) by $\zeta_l^m=-l(l+1)\psi_l^m$ and $D_l^m=-l(l+1)\chi_l^m$.

The expansions for the diagnostic quantities U and V are given in *I*.

written as

$$\zeta(\phi,\lambda,t)=\sum_{m=-J}^{J}\sum_{l=|m|}^{|m|+J}\zeta_l^m(t)Y_l^m(\phi,\lambda), \tag{4}$$

$$D(\phi,\lambda,t)=\sum_{m=-J}^{J}\sum_{l=|m|}^{|m|+J}D_l^m(t)Y_l^m(\phi,\lambda), \tag{5}$$

$$\Phi(\phi,\lambda,t)=a^2\sum_{m=-J}^{J}\sum_{l=|m|}^{|m|+J}\Phi_l^m(t)Y_l^m(\phi,\lambda), \tag{6}$$

and with Φ_s being expanded in an identical manner to Φ. In the above $Y_l^m(\phi,\lambda)=P_l^m(\sin\phi)e^{im\lambda}$; $P_l^m(\sin\phi)$ is an associated Legendre polynomial of degree l and order m normalized to unity; and J is the (rhomboidal) truncation parameter, m denoting a planetary wavenumber and $(l-m)$ a meridional wavenumber. When the above expansions are substituted in (1)–(3), the resulting equations, in the form of ordinary differential equations [Eqs. (21), (23), (24) of I], can be readily integrated. Full details of the computational methods employed are given in I.

The model, incorporating a semi-implicit algorithm (Robert 1969), was integrated with the geopotential height and divergence coefficients restricted to be symmetric ($l-m$, even) and the vorticity coefficients restricted to be anti-symmetric ($l-m$, odd); such a choice constrains the calculation to be hemispheric.

3. The initial data

The GARP basic data set for November 1969 was the most comprehensive set of Southern Hemisphere data available; a detailed description of the manual techniques employed in the preparation of the analyses is given by Phillpot *et al.* (1971), and Thompson (1972) gives a detailed discussion of the data network available for the analyses. The manually prepared charts (mean sea level and 500 mb) for the period 3–16 November 1969 were digitized and the resulting product used as input to a numerical analysis scheme which ensures vertical consistency and gross balance. The resulting grid-point values of 500 mb geopotential and wind components (on a regular 47×47 stereographic projection grid) were then interpolated to a latitude-longitude grid prior to spherical harmonic analysis using a technique similar to that of Eliasen and Machenhauer (1965). Further details of the analysis technique can be found in Appendix C of Bourke (1974).

4. Diagnostic quantities

For notational convenience we define a quantity

$$\Delta\Phi=\Phi_1-\Phi_2, \tag{6}$$

where Φ_1 and Φ_2 are two fields (e.g., geopotential height) to be compared. Then the mean square error σ^2 between the two fields can be written as

$$\sigma^2=\frac{1}{4\pi}\int_0^{2\pi}\int_{-\pi/2}^{\pi/2}(\Delta\Phi)^2\cos\phi d\phi d\lambda. \tag{7}$$

Writing the spectral expansion of the difference fields $\Delta\Phi$ as

$$\Delta\Phi=a^2\sum_{m=-J}^{J}\sum_{l=|m|}^{|m|+J}(\Delta\Phi)_l^m P_l^m(\sin\phi)e^{im\lambda}, \tag{8}$$

and substituting this into (7) yields

$$\sigma^2=\frac{a^4}{2}\sum_{m=-J}^{J}\sum_{l=|m|}^{|m|+J}(\Delta\Phi)_l^m(\Delta\phi)_l^{m*}, \tag{9}$$

where the asterisk represents a complex conjugate. Note that since (9) is a double summation over all allowed values of the wavenumbers m and l, it is a simple matter to calculate the contribution to the total mean square error from a particular planetary wavenumber m:

$$\sigma_m{}^2=\frac{a^4}{2}\sum_{l=|m|}^{|m|+J}(\Delta\Phi)_l^m(\Delta\Phi)_l^{m*}. \tag{10}$$

Two methods of presenting the distribution of mean square error in the physical domain have been chosen. The first method gives the contribution to the total mean square error as a function of latitude. The second method gives the mean square error in three equal-area sectors of the hemisphere.

For the purposes of this study it was decided that only a very simple measure of "skill" in a prognosis was necessary; a model prognosis was considered to have skill when the mean square error in the prognosis was smaller than the error in the corresponding prognosis based on persistence alone.

Another readily derivable quantity, the spectrum of kinetic energy, is useful both as a measure of model performance and as a diagnostic of the state of the atmosphere:

$$K_m=\frac{a^2}{3}\sum_{l=|m|}^{|m|+J}(\zeta_l^m\zeta_l^{m*}+D_l^mD_l^{m*})/[l(l+1)],\quad l\neq 0. \tag{11}$$

5. Methodology of the forecast experiments

Two basic types of experiment were conducted. In one the aim was to determine the sensitivity or otherwise of a particular forecast to variations in the external parameters of the model. For each forecast the initial data remained constant (500 mb geopotential height and vorticity fields for 0000 GMT 3 November 1969) but one or other of time step, truncation wavenumber, or method of initialization was altered. Usually only 48 h prognoses were computed.

Having determined the sensitivity of the model to various parameters, experiments of the second type

were then conducted. The aim of this type was to clarify the capability of the model as a forecasting aid. All external parameters were kept constant and the model was initialized with data from ten successive days (3 November 1969 to 12 November 1969) and prognoses for 24, 48, 72 and 96 h were produced.

6. Variation in external parameters—results

a. Size of time step

Errors from time truncation were found to be very small. The rms difference between the geopotential height fields computed using time steps of 900 and 3600 s was less than 1.2 m after 72 h of integration. Hence the convenient time step of 3600 s was chosen for all subsequent experiments.

b. Variation in resolution

Using the same initial data (for 0000 GMT 3 November 1969) represented by a set of spherical harmonic coefficients with rhomboidal truncation with $J=15$, three forecasts were made using a different truncation for each integration, *viz* $J=15$, $J=21$ and $J=30$. These truncations correspond to 248, 473 and 945 degrees of freedom in the geopotential amplitudes, respectively. The 48 h prognoses obtained from each of three truncation parameters differ very slightly on visual evaluation of the charts; the hemispheric rms error in the height of the 500 mb surface of the prognoses compared to the observed data at 0000 GMT 5 November 1969 were 65.9 m ($J=15$), 64.1 m ($J=21$) and 64.7 m ($J=30$).

The differences between the prognoses with different resolutions can perhaps be better presented as mean square differences between the geopotential heights from two pairs of results; $J=15$ compared to $J=30$, $J=21$ compared to $J=30$. Fig. 1 shows this difference for each pair of 48 h prognoses for each planetary wavenumber from 1 to 30. The differences occur mainly in the low planetary wavenumber range 1 to 10. Integrated over the entire spectrum the rms difference was 19.4 m for $J=15$ compared to $J=30$, 9.8 m for $J=21$ compared to $J=30$, and 20.6 m for $J=15$ compared to $J=21$. Although these differences between 48 h prognoses with different resolutions suggest that improved numerical accuracy is achieved with higher resolution there is little evidence to suggest that the skill of a prognosis is improved with a higher resolution. Deficiencies in the dynamical processes represented in the model were not compensated for by the increased numerical accuracy in the calculation of those processes which are allowed.

It was decided on the basis of the above results that prognoses made at truncation $J=15$ were adequate for these data. The additional computational time required for higher resolution was not warranted in view of only a slight gain in skill.

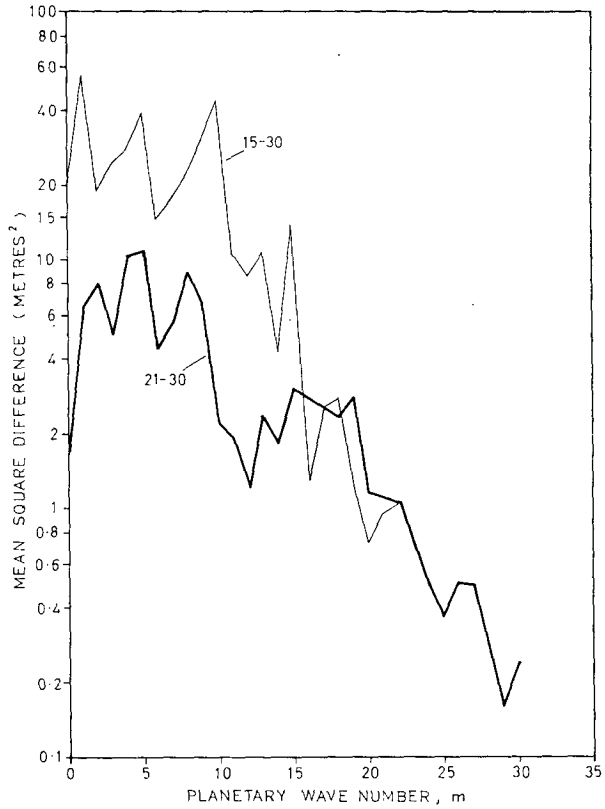

FIG. 1. Variation with planetary wavenumber of the mean square difference between the 48 h geopotential height fields computed by the spectral model with different resolutions. The heavy line shows the difference between the prognosis with $J=21$ and $J=30$, and the thin line the difference between prognoses with $J=15$ and $J=30$. The initial fields used were as analyzed at 0000 GMT 3 November 1969.

Puri and Bourke (1974) have conducted a much more extensive truncation study using different initial data. Their study concentrated on the numerical accuracy of the solution and the truncation results reported here are consistent with their results provided that allowance is made for the higher levels of variance in the IGY data used in their study.

c. Variation in mean height of the free surface

As discussed by Cressman (1958) the divergence generated can modify the tendency for excessive retrogression of the long-wave component. Since the lower the mean height of the free surface the greater the amount of divergence generated, some effect on the skill in the resulting prognoses is to be expected. Four different heights were used: 11.8 m, 5.6 km, 2.8 km and 1.4 km; as the height was decreased some slight improvement in skill was found concentrated in the low wavenumber portion of the spectrum. The change in the rms error in a 48 h prognosis from 3 November 1969 with variation in the mean height is presented in

TABLE 1. Root mean square error (m) in 48 h prognoses from 0000 GMT 3 November 1969 with various mean free heights.

Height of free surface (km)	rms error in prognoses (m)
11.8	68.2
5.6	65.9
2.8	64.8
1.4	63.6

Table 1—the error decreases from 65.9 with 5.6 km height to 63.6 m with 1.4 km height.

With the lack of any compelling reason to vary the mean height of the free surface far from the typical height of the 500 mb surface, the mean height was left at 5.6 km in the remaining experiments.

d. Inclusion of orography

A symmetric set of spectral coefficients representative of the Southern Hemisphere land masses has been computed (McAvaney, 1974) from smoothed values of the 5°×5° average land elevation data of Lee and Kaula (1967). The smoothing is such that the average height of the Antarctic plateau is reduced to 1.9 km. These coefficients were incorporated into the spectral model and a 48 h prognosis computed (with 5.6 km mean height) from the initial data for 3 November 1969. Compared to the prognosis with no orography the major changes occurred over latitudes south of 55°S due to the dominant land mass of the Antarctic continent. In the presence of orography, high-latitude troughs lagged their counterparts in the no-orography case. The phase changes were sufficient to increase the rms error in the 48 h prognosis to 73.1 m (compared to 65.9 m for the no-orography case) with the main increase in error being associated with wavenumbers 1 and 2.

The retardation in movement of high-latitude systems is attributed in part to the influence of latitudinal gradients of the orography. A linear analysis of this type of problem has been made by Veronis (1966) who has demonstrated that such latitudinal orographic gradients are dynamically equivalent to the variation of the Coriolis parameter with latitude so that the phase speed of Rossby waves depends on both gradients. With the particular smoothed orography used in the above prognosis, it is only in the vicinity of the Antarctic continent that latitudinal gradients in the orography are large enough to significantly modify the phase speed of the Rossby waves.[2] Longitudinal gradients in orography may superimpose perturbations on predominantly zonal flow but these are not apparent from visual inspection of the above prognosis.

[2] At 60°S the latitudinal gradient in the Coriolis parameter is 1.14×10^{-11} m^{-1} s^{-1} compared to 2.5×10^{-11} m^{-1} s^{-1} for a typical value of the corresponding orographic gradient term for 5.6 km mean height; hence some retardation in phase speed would be expected.

Since no improvement in overall skill of a prognosis could be found when orography was included, no-orography was used in subsequent experiments. However, further investigation of the effect of orography on Southern Hemisphere prognoses would seem desirable.

e. Initialization

It was found from quite early experiments that the model was computationally stable when initialized directly with the vorticity, divergence and geopotential height fields as analyzed, and furthermore that no small-scale gravity wave activity was generated during the course of an integration. However, such a simple approach to initialization gave unrepresentative prognosis fields at low latitudes due to the generation of spurious divergence by the model at these latitudes. The most suitable method of initialization found was to use the vorticity and geopotential height fields as analyzed but to set the divergence field identically zero at the start of the integration. Other methods of initialization, including the use of the linear and nonlinear balance equations as well as dynamic initialization, did not give any marked improvement in the prognoses.

An extremely large-scale axisymmetric inertio-gravitational wave was generated during each integration and appeared principally in the Φ_2^0 and D_2^0 components regardless of the method of initialization used. Such a large-scale oscillation is apparent in many primitive equation hemispheric and global models and in general is unrelated to the much smaller scale shorter period gravity wave oscillations which are discussed in many descriptions of initialization procedures (e.g., Winninghoff, 1973; Temperton, 1973). This large-scale oscillation is discussed further in Section 9 where it is demonstrated that the presence of this oscillation does not lead to a deterioration in skill.

7. An example of a prognosis made with the spectral model

The 500 mb geopotential height field for 0000 GMT 3 November 1969 used to initialize the model in one experiment is shown in Fig. 2a. The resulting 48 h geopotential height prognostic is shown in Fig. 2b[3] and the verifying geopotential height field (for 0000 GMT 5 November 1969) is shown in Fig. 2c.

The model has produced a quite successful prognosis over the Australian region and over the western Pacific. Deficiencies in the prognosis are apparent, especially over the Indian Ocean to the southwest of Australia where the movement of the cutoff low has been too slow. This prognosis is also somewhat deficient in retaining excessive amplitude in the trough at 90°W and in

[3] Details of the external parameters used in this prognosis were as follows: truncation, $J=15$; time-step, 3600 s; mean height of free surface, 5.6 km.

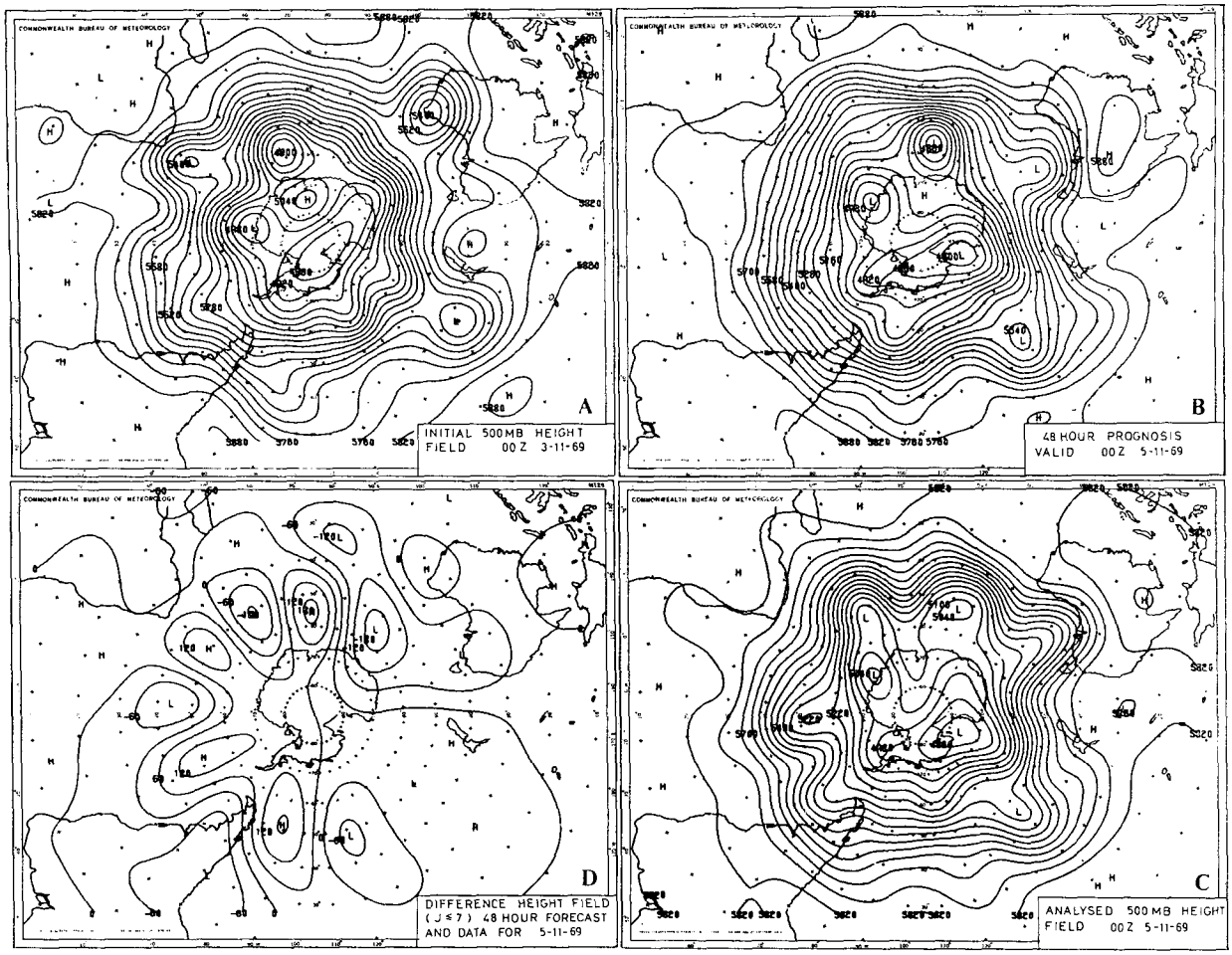

FIG. 2. 500 mb geopotential height (m) fields: (a) as analyzed at 0000 GMT 3 November 1969, contour interval 60 m; (b) 48 h prognoses valid at 0000 GMT 5 November 1969 computed using spectral model; (c) verification analysis at 0000 GMT 5 November 1969; (d) difference field between (b) and (c), contour interval 60 m. All difference amplitudes corresponding to truncation $J \geqslant 8$ have been suppressed.

producing too zonal a flow over the South Atlantic. These larger scale features are apparent in the difference field of Fig. 2d where the geopotential height difference between the 48 h prognosis and the verifying analysis has been plotted for wavenumbers 0 to 7 only.

In evaluating such a prognosis it is of course expected that major deficiencies will occur in substantially data-sparse areas; the comments of Phillpot *et al.* (1971) regarding the reliability of the data are cautionary in this respect.

A detailed investigation of the spatial and spectral distribution of errors apparent from a visual inspection of the prognosis and verifying charts is given in the following section.

8. Spatial and spectral distribution of the mean square error

Since the hemispheric mean square error is often used as a measure of skill for a given forecast whereas in practice one is often more concerned with a somewhat restricted range of latitudes and longitudes, it is important to know how representative a hemispheric mean square error can be. This will be illustrated below for a 48 h prognosis from 0000 GMT 3 November verifying at 0000 GMT 5 November; the conclusions apply to other cases.

The rms error over the entire hemisphere for the 48 h prognoses of geopotential height (shown in Fig. 2c) is 65.9 m compared to 92.4 m for the rms error for the persistence or "no change" forecast. Fig. 3 illustrates how the contribution to the overall mean square forecast and persistence errors vary with latitude.[4] Approximately 90% of the total mean square error for both forecast and persistence curves is contributed by

[4] The third curve in both Figs. 3 and 4 shows the variation in mean square error for a prognosis in which the large-scale oscillation first discussed in Section 6e is suppressed using the technique described in Section 9.

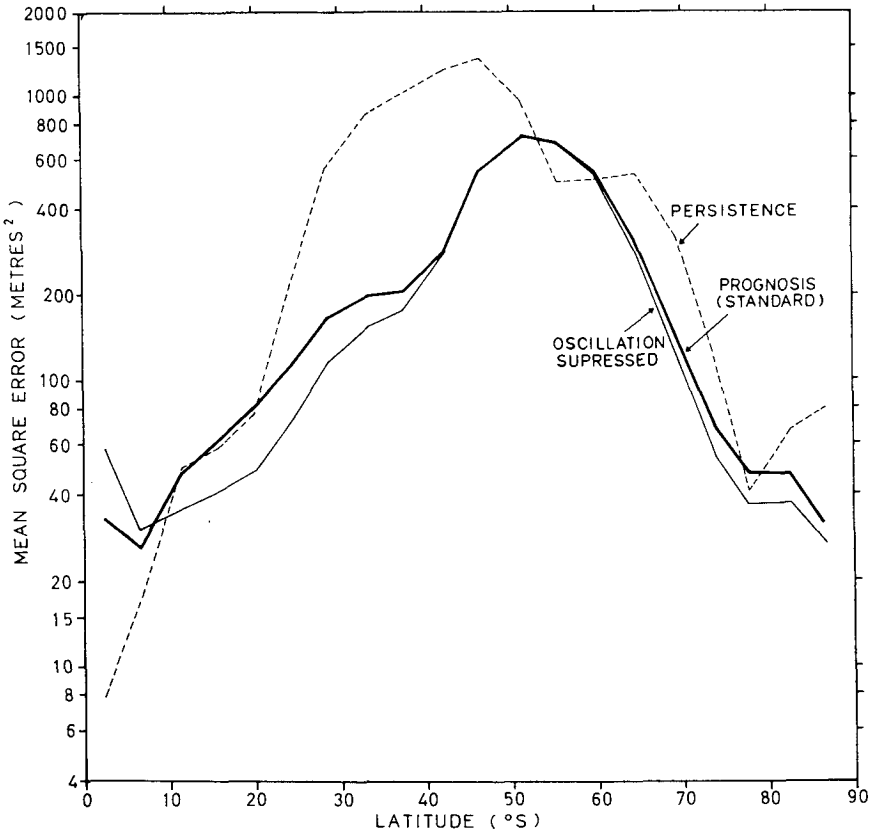

FIG. 3. Variation with latitude of the mean square error difference for a 48 h model prognosis from 0000 GMT 3 November 1969 verifying at 0000 GMT 5 November 1969 (heavy line) and 48 h persistence prognosis using data for 3 November 1969 (dashed line). The thin line was obtained from a similar prognosis in which the large-scale inertio-gravitational wave present in the other prognosis is suppressed.

latitudes 25°S to 75°S; moreover, for most of this region (the exception being near 55°S) the forecast error curve is considerably below the persistence error curve. Hence the improvement of 26.5 m in the value of the hemispheric mean error in the prognosis compared to persistence occurs mainly in mid-latitudes.

Corresponding to the distribution of mean square error with latitude, Fig. 4 shows the distribution of the mean square error with planetary wavenumber. The major contribution to the total mean square error in the prognosis (~93%) is from planetary wavenumbers less than 10; in addition, the model prognosis is better than persistence for wavenumbers greater than 2. Less than 7% of the total error is contributed by planetary wavenumbers greater than 11 and hence the improvement of the model prognosis over persistence at high wavenumbers may not be significant.

An attempt to give some measure of the variations in the difference field over various regions of the hemisphere has been made by selecting three sectors each covering 120° of longitude and from equator to pole. The distribution of the rms error in geopotential height (m) for both the 48 h prognosis and persistence forecast for the three sectors is shown in Table 2.

Region II, which encompasses a large area of the relatively well-forecast fields over the Pacific Ocean, has the smallest absolute rms error in the forecast; however, in terms of improvement over persistence Region I, which includes the area over the Australian continent, displays greater skill despite the large contribution to the absolute rms error due in part to the prognosis failure to the southwest of the continent.

9. Effect of a large-scale oscillation on verification

In common with many other primitive equation hemispheric and global numerical models (e.g., Miyakoda *et al.*, 1969; Gilchrist *et al.*, 1973) a large-scale axisymmetric inertio-gravitational wave was present in all integrations of the spectral model discussed hitherto. In the present model the oscillation is apparent in the time variation of the hemispheric kinetic energy which had a quasi-periodicity of about 11.0 h. While the presence of such an oscillation is clearly undesirable, the effect on forecast skill nevertheless appeared small. Hence after initial attempts at suppressing the oscillation through standard initialization techniques proved unsuccessful, it was decided to

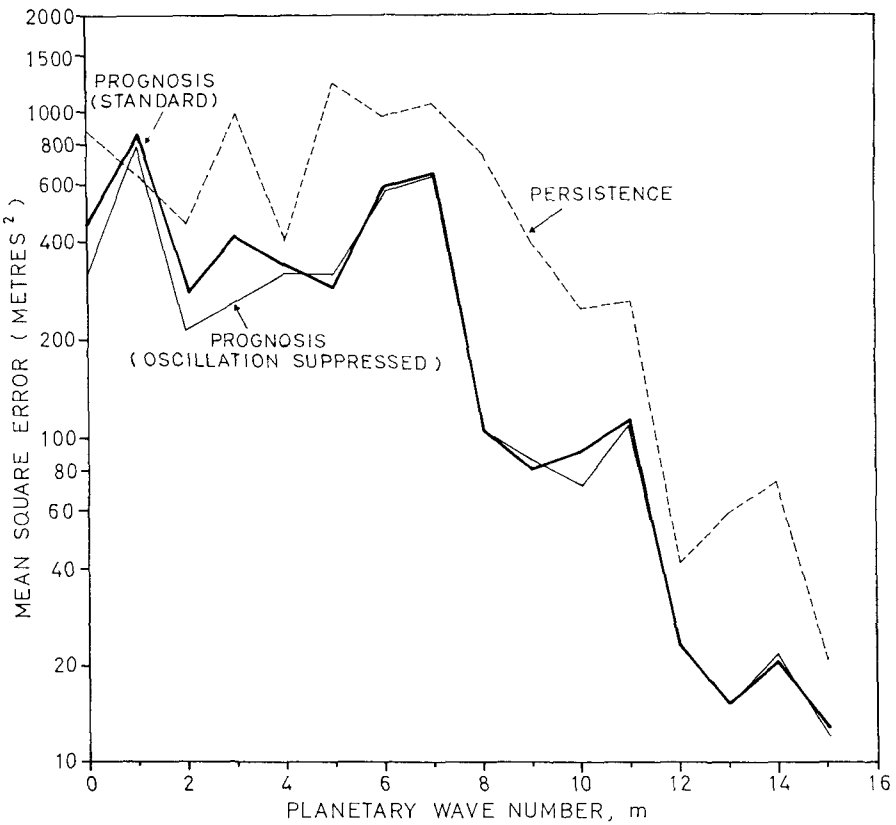

FIG. 4. As in Fig. 3 except for variation with planetary wavenumber.

proceed with the prognoses regardless of the presence of the oscillation. Evidence presented below offers some justification for this pragmatic approach.

After the major computational portions of this study had been completed, Bourke (1974) found that the use of a divergence dissipation term in a similar manner to the divergence diffusion term proposed by Sadourny (1972) successfully suppressed the large-scale oscillation in a multi-level spectral model and subsequently was also successful in the single-level model as used in this study. Rather than repeat the earlier computations it was decided to simply demonstrate the effect of the suppression of the oscillation on the verification scores for one particular prognosis.

TABLE 2. Comparison of rms errors (m) in the 48 h numerical prognosis from 0000 GMT 3 November 1969, with the persistence forecast for each of three sectors over the hemisphere.

Region	Numerical prognosis	Persistence	Improvement
I (75°E–162.5°E)	73	104	31
II (165°E–47.5°W)	58	76	18
III (45°W–72.5°E)	65	94	29
Whole	66	92	26

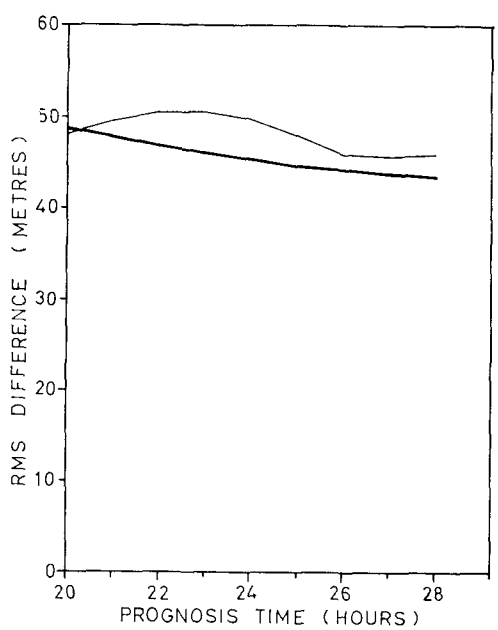

FIG. 5. The rms difference in geopotential height between a prognosis at various times after initialization (0000 GMT 3 November 1969) and observed data at 0000 GMT 4 November 1969. The thin line is for the standard prognosis with the large-scale oscillation present and the heavy line is for a prognosis with the oscillation suppressed.

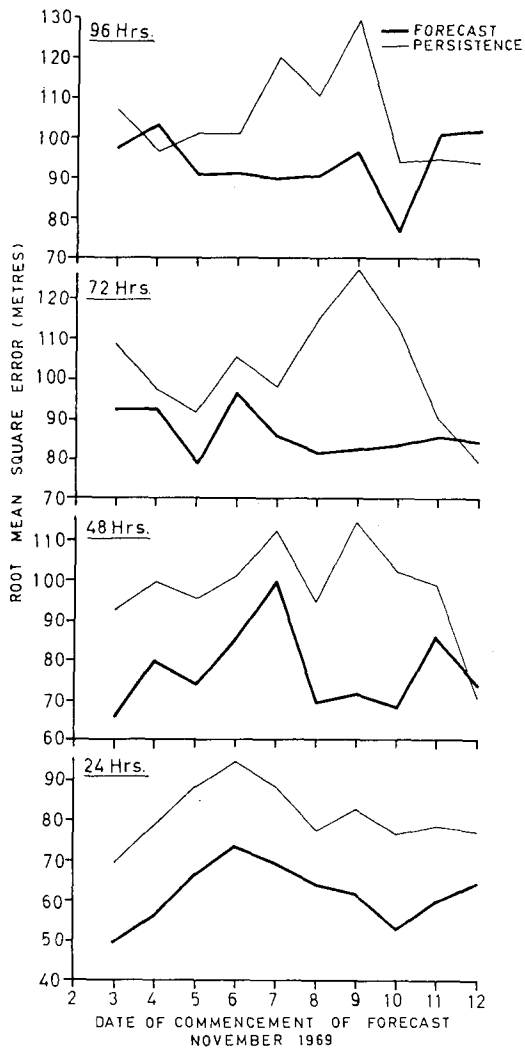

FIG. 6. The day-to-day variation of the hemispheric rms error in the model prognoses (heavy lines) and persistence prognoses (thin lines) for 24, 48, 72 and 96 h, respectively, ahead of the commencement dates.

Fig. 5 shows the variation of the rms difference between prognoses at hourly intervals a few hours either side of the verification time. The difference between the two curves (with and without the oscillation) is relatively small, with the variation in the curve obtained in the presence of the oscillation being small compared to the mean over the time interval shown.

The effect of suppression of the oscillation on the distribution of the mean square error with latitude and planetary wavenumber are shown in Figs. 3 and 4, respectively. In general, suppression of the oscillation has resulted in slight improvement; the only changes of any importance occur at low latitudes (equatorward of 30°S) and high latitudes (poleward of 70°) with corresponding main changes in planetary wavenumbers 0 to 2.

TABLE 3. Average rms error (m) in height of 500 mb surface over 10 forecasts from 0000 GMT 3 November 1969 to 0000 GMT 12 November 1969 and forecasts of 24, 48, 72 and 96 h forecasts.

	24 h	48 h	72 h	96 h
Numerical forecast	62	77	86	94
Persistence forecast	81	98	103	105

The results discussed above, while admittedly for only one set of initial data, indicate that the presence of an oscillation in a prognosis does not cause a major increase in the mean square error. This conclusion is considered general for all prognoses since initializing the model with data for 6 November 1969 (which gave the worst 24 h forecast) and recalculating a 24 h prognosis with the oscillation suppressed produced a forecast which was only slightly better (in terms of rms error) than the original with the improvements occurring over a similar range of latitudes and planetary wavenumbers as the above.

10. Day-to-day and averaged statistics

a. Errors in geopotential height

A total of ten model prognoses were made with the values of the external parameters as discussed earlier in Section 6. Root mean square errors in geopotential height for each of these numerical prognoses (24, 48, 72 and 96 h) were computed using Eq. (9) and then averaged over all prognoses. A similar procedure was used with regard to persistence forecasts. The day-to-day variation in these two error quantities for each of the 24, 48, 72 and 96 h forecasts is shown in Fig. 6. The average values over the 10-day period are given in Table 3.

It is apparent from Fig. 6 that the spectral model gives a better forecast of geopotential height than does persistence for at least two, and possibly three, days ahead. At 48 h there is only one day for which the improvement of the spectral model forecast over persistence was less than 10 m, and at 72 h four model forecasts show less than 10 m improvement over persistence.

Since from Table 3 and Fig. 6 some skill is evident at 48 h it is worth considering the distribution of this skill over the hemisphere and with planetary wavenumber. The geopotential variation of the rms error on a day-to-day basis is presented in Fig. 7 by using the average errors in each of the three sectors defined earlier in Section 8. In general some skill is displayed in all sectors with noticeably poor skill in Region II for the prognosis initialized with data for 6 November 1969 and in Region III for the prognosis initialized on the following day. Inspection of the original manually prepared MSL and 500 mb charts revealed that extensive

TABLE 4. Average rms error (m) at 48 h over a 10-day period in three sectors.

	Region I	Region II	Region III
Numerical forecast	76.3	67.8	83.2
Persistence forecast	90.2	85.9	111.8

baroclinic development occurred near the Antarctic peninsula and over the South Atlantic during the period 7 to 9 November 1969 so it is not surprising that the regional errors for the one-level model were large around these dates. The poor skill evident in Region I for the prognoses initialized with data for 11 and 12 November was due mainly to the inability of the model to predict the behavior of a complex system of troughs near the Antarctic coast. In general, however, the more consistent skill shown in Region I could be expected due to the more extensive conventional data network encompassed by the region. It is apparent that the hemispheric rms errors only partially reflect these deficiencies in the model prognoses.

It is interesting to compare the average root mean square errors for the one-level spectral model at 24 and 48 h (62 m and 77 m, respectively) with typical errors from an operational finite-difference barotropic model using the more extensive data of the Northern Hemisphere. In the report of the National Meteorological Center (1971) the average rms error over the hemisphere for the month May 1971 was given as 45.1 m for a 36 h prognosis with persistence error being 63.5 m. The larger persistence error in the Southern Hemisphere (98 m at 48 h) may reflect the sparsity of data or more rapid evolution of systems.

The distribution with latitude of the average mean square error in all 48 h prognoses of geopotential height is shown in Fig. 8. The average error in the model prognoses shown by the solid line is less than the average error in all persistence prognoses as shown by the thin line over the mid-latitude range 30°S to 60°S. Fig. 9 shows the average mean square error plotted in the spectral domain. Again the average of the model prognoses (solid line) shows improvement over persistence (thin line) for most of the spectrum but with the main contribution to this improvement being due to the wavenumber range 3 to 9 (the wavenumber range over which the most rapid changes can occur, both in the model and as diagnosed from observed data).

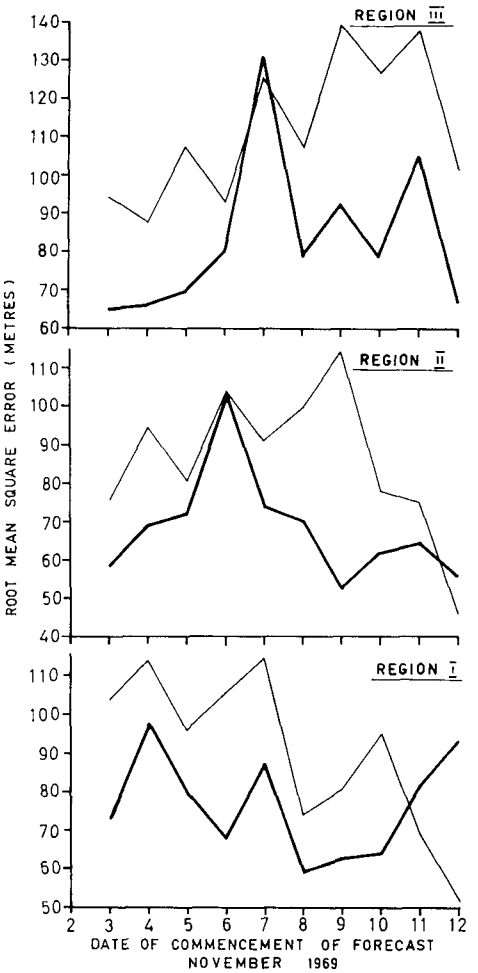

FIG. 7. The day-to-day variation of the root mean square error (meters) over three sectors of the hemisphere for 48 h model (heavy lines) and persistence (thin lines) prognoses from the commencement dates shown.

b. Vorticity error

Since vorticity is one of the predicted quantities with the spectral model, it is appropriate to present the rms vorticity errors particularly in view of the fact that contributions to the spectrum of vorticity from high wavenumbers can be comparable to that from low wavenumbers.

The day-to-day variation in the rms vorticity error is shown in Fig. 10. Similar trends to the geopotential error curves are apparent, with the spectral model being capable of forecasting the vorticity field better than persistence up to about 48 h. For times greater than this, persistence provides as good or a better forecast on about half the occasions.

It is to be noted that the day-to-day variations in the rms vorticity errors presented here are very similar to those for 24 and 48 h prognoses computed by a more sophisticated multi-level spectral model using the same initial data (Bourke, 1974).

c. Kinetic energy spectrum

The spectrum of observed kinetic energy computed using Eq. (13) and averaged over the 10-day period

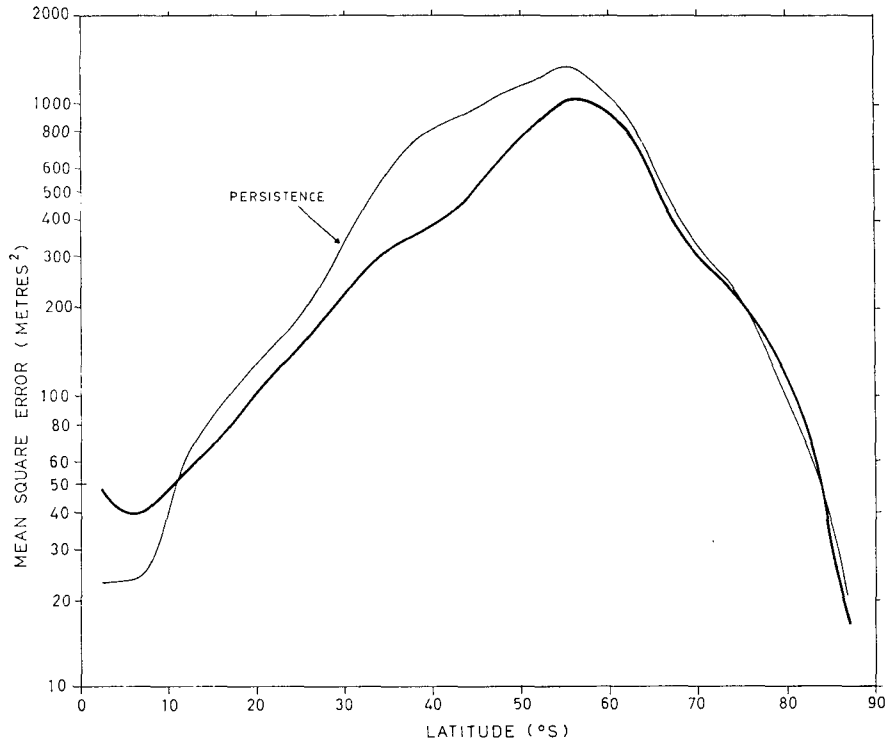

FIG. 8. The distribution with latitude of the average mean square error in geopotential height for all 48 h prognoses (10) made with spectral model (heavy line) compared to the average mean square error in the persistence prognoses (thin line).

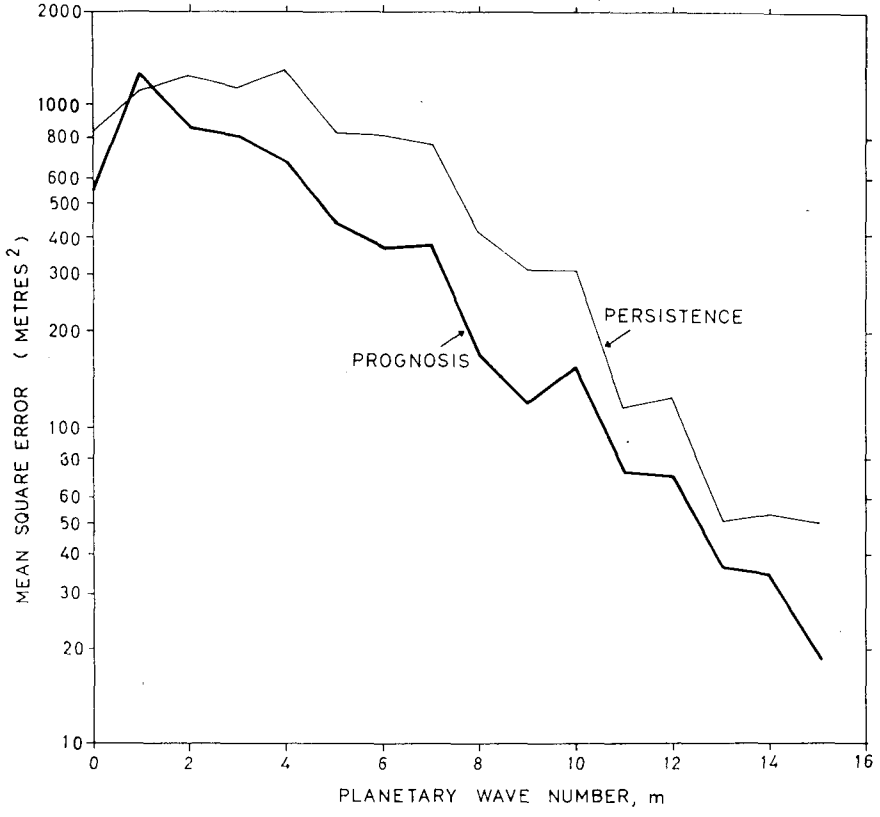

FIG. 9. The distribution with planetary wavenumber of the average mean square error in geopotential height for all 48 h model prognoses (heavy line) compared to the average mean square error in the persistence prognoses (thin line).

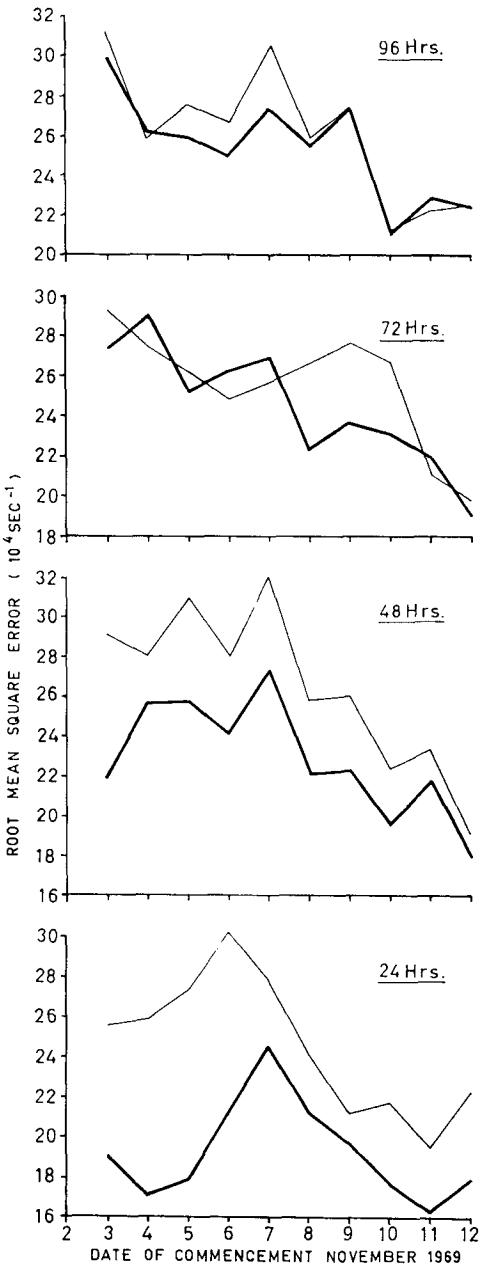

FIG. 10. The day-to-day variation of the hemispheric rms error in vorticity for model (heavy lines) and persistence prognoses (thin lines) for 24, 48, 72 and 96 h ahead of the commencement dates.

is contrasted with the average of the 48 h model prognoses in Fig. 11. The amplitude of the components of the observed kinetic energy at planetary wavenumbers 3 and 7 were significant over the period. Compared to the observed data, the spectrum from the model results shows a deficiency in kinetic energy over the middle portion of the spectrum accompanied by an increase at low wavenumbers 1 and 0 (the latter is given in the lower portion of the diagram because of the

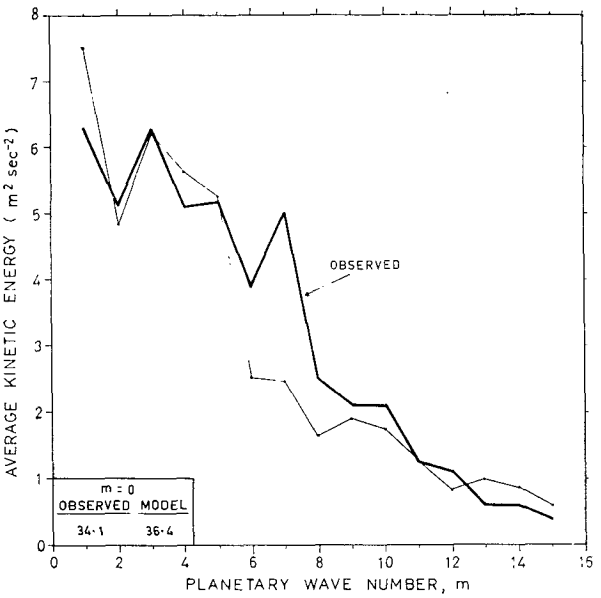

FIG. 11. Average kinetic energy for observed data over the period 3 to 12 November 1969 (heavy line) compared to the average kinetic energy for 48 h model prognoses (thin line).

large magnitude); the slight excess of kinetic energy at high wavenumbers for the model is most probably symptomatic of spectral blocking effects (Puri and Bourke, 1974).

The tendency for the zonal component ($m=0$) of the kinetic energy to increase with time is characteristic of a barotropic model and is associated with the energy cascade process of Fjortoft (1953). The effect of the excess in mean zonal kinetic energy on the model prognoses can perhaps be more readily seen in Fig. 12 where the time average of the observed and model mean zonal wind components have been plotted against latitude. Over the middle latitude range 40°S to 55°S

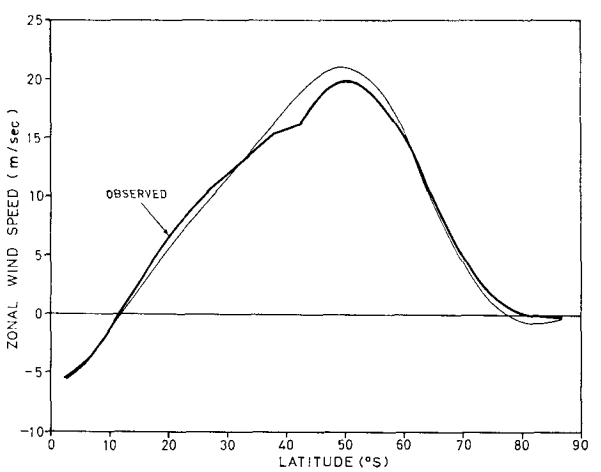

FIG. 12. Average zonal wind speed profile for observed data over the period 3 to 12 November 1969 (heavy line) compared to the average zonal wind speed profile for the 48 h model prognoses (thin line).

differences in the two zonal mean quantities reach as much as 5 m s^{-1}.

11. Summary and conclusions

Several days of the Southern Hemisphere November 1969 GARP 500 mb data set have been used to initialize a one-level primitive equation spectral model. The model of initialization employed was to set the divergence field identically zero at the start of the integration; this method controls the higher wavenumber external gravity wave modes quite well. Although a large-scale inertio-gravitational oscillation appeared during the course of the integrations, no appreciable deterioration in quality of the prognoses occurred; the divergence dissipation scheme of Bourke (1974) has since been shown to suppress the oscillation.

The model has proved relatively insensitive to variation in external parameters. In particular, the use of wavenumber 15 truncation for the prognoses proved to be adequate, with the increased numerical accuracy with higher wavenumber truncation not producing better quality prognoses. Reduction of the mean height of the free surface from the standard value of 5.6 km only marginally improved the quality of the prognoses with the main reduction being in the mean square error at low wavenumbers.

When orography was included in the model the quality of the prognosis deteriorated due to excessive phase lags in high-latitude systems. We consider this is due in part to the larger values of the latitudinal gradient in the orography at these latitudes as outlined by Veronis (1966).

The day-to-day values of the hemispheric rms error in the 48 h model prognoses are consistently better than those for persistence prognoses; over the 10-day period the average gain for the entire hemisphere of the model prognoses over persistence was 21 m. The distribution of mean square error with latitude and planetary wavenumber shows that this gain over persistence occurs over the mid-latitude range 30°S–60°S and for wavenumbers 3 to 9.

Acknowledgments. The authors wish to acknowledge the assistance of Mr. R. Thurling and Miss L. Clear whose able programming greatly assisted the progress of this work. Also the authors wish to thank Mr. G. Kelly who provided the digitized GARP data and Mr. R. Seaman who generated the numerical grid-point analyses. The time given in informative discussions of this work by Mr. P. Noar and Dr. K. Puri is much appreciated.

REFERENCES

Bourke, W., 1972: An efficient one-level primitive equation spectral model. *Mon. Wea. Rev.*, **100**, 683–689.

——, 1974: A multi-level spectral model. I. Formulation and hemispheric integrations. *Mon. Wea. Rev.*, **102**, 687–701.

Cressman, G. P., 1958: Barotropic divergence and very long atmospheric waves. *Mon. Wea. Rev.*, **86**, 293–297.

Eliasen, E., and B. Machenhauer, 1965: A study of the fluctuations of the atmospheric planetary flow patterns represented by spherical harmonics. *Tellus*, **17**, 220–238.

Fjortoft, R., 1953: On the changes in the spectral distribution of kinetic energy for two-dimensional, nondivergent flow. *Tellus*, **5**, 225–230.

Gilchrist, A., G. A. Corby and R. L. Newson, 1973: A numerical experiment using a general circulation model of the atmosphere. *Quart. J. Roy. Meteor. Soc.*, **99**, 2–34.

Lee, W. H. K., and W. M. Kaula, 1967: A spherical harmonic analysis of the earth's topography. *J. Geophys. Res.*, **72**, 753–758.

Miyakoda, K., J. Smagorinsky, R. F. Strickler and G. D. Hembree, 1969: Experimental extended predictions with a nine-level hemispheric model. *Mon. Wea. Rev.*, **97**, 1–76.

McAvaney, B. J., 1974: On spherical harmonic analysis of topography. (To be published).

National Meteorological Center, 1971: Numerical weather prediction activities: First half 1971. National Weather Service, NOAA, Silver Spring, Md., 40 p.

Phillpot, H. R., P. G. Price, N. B. Neal and F. A. Lajoie, 1971: GARP basic data set analysis project: The first experiment—November 1969. *Aust. Meteor. Mag.*, **19**, 48–81.

Puri, K. K., and W. Bourke, 1974: Implications of horizontal resolution in spectral model integrations. *Mon. Wea. Rev.*, **102**, 333–347.

Robert, A., 1969: Integration of a spectral model of the atmosphere by the implicit method. *Proc. WMO/IUGG Symp. Numerical Weather Prediction*, Tokyo, 26 November–4 December 1968, Jap. Meteor. Agency, Tokyo, VII-19 to VII-24.

Sadourny, R., 1972: Forced geostrophic adjustment in large scale flow. Laboratoire de Meteorologie Dynamique de C.N.R.S., France (unpublished manuscript).

Temperton, C., 1973: Some experiments in dynamic initialization for a simple primitive equation model. *Quart. J. Roy. Meteor. Soc.*, **99**, 303–319.

Thompson, T., 1972: The Basic Data Set Project. GARP Publ. Ser. No. 9, GARP WMO/ICSU Joint Organising Committee, WMO, Geneva.

Veronis, G., 1966: Rossby waves with bottom topography. *J. Marine Res.*, **24**, 338–349.

Voice, M. E., U. Radok, D. Jenssen and J. Bayliss, 1972: A barotropic numerical weather prediction experiment for the Australian region. *Aust. Meteor. Mag.*, **20**, 129–173.

Winninghoff, F. J., 1973: Note on a simple, restorative-iterative procedure for initialisation of a global forecast model. *Mon. Wea. Rev.*, **101**, 79–84.